



# Data-driven stochastic inversion via functional quantization

Mohamed Reda El Amri<sup>1,2</sup> · Céline Helbert<sup>3</sup> · Olivier Lepreux<sup>4</sup> · Miguel Munoz Zuniga<sup>1</sup> · Clémentine Prieur<sup>2</sup> · Delphine Sinoquet<sup>1</sup>

Received: 27 July 2018 / Accepted: 6 August 2019  
© Springer Science+Business Media, LLC, part of Springer Nature 2019

## Abstract

In this paper, we propose a new methodology for solving stochastic inversion problems through computer experiments, the stochasticity being driven by a functional random variables. This study is motivated by an automotive application. In this context, the simulator code takes a double set of simulation inputs: deterministic control variables and functional uncertain variables. This framework is characterized by two features. The first one is the high computational cost of simulations. The second is that the probability distribution of the functional input is only known through a finite set of realizations. In our context, the inversion problem is formulated by considering the expectation over the functional random variable. We aim at solving this problem by evaluating the model on a design, whose adaptive construction combines the so-called stepwise uncertainty reduction methodology with a strategy for an efficient expectation estimation. Two greedy strategies are introduced to sequentially estimate the expectation over the functional uncertain variable by adaptively selecting curves from the initial set of realizations. Both of these strategies consider functional principal component analysis as a dimensionality reduction technique assuming that the realizations of the functional input are independent realizations of the same continuous stochastic process. The first strategy is based on a greedy approach for functional data-driven quantization, while the second one is linked to the notion of space-filling design. Functional PCA is used as an intermediate step. For each point of the design built in the reduced space, we select the corresponding curve from the sample of available curves, thus guaranteeing the robustness of the procedure to dimension reduction. The whole methodology is illustrated and calibrated on an analytical example. It is then applied on the automotive industrial test case where we aim at identifying the set of control parameters leading to meet the pollutant emission standards of a vehicle.

**Keywords** Functional random variable · Karhunen–Loève expansion · Data reduction · Functional quantization · Set estimation · Gaussian process models

## 1 Introduction

In recent years, computer models are omnipresent in engineering and sciences, because the corresponding physical experimentation is costly or even impossible to execute. Indeed, numerical simulations are often used to replace physical experiments as underlined in Bect et al. (2012) and

Chevalier et al. (2014b). Practitioners are interested not only in the response of their model for a given set of inputs (forward problem) but also in recovering the set of input values leading to a prescribed value or range of the output of interest. The problem of estimating such a set is called hereafter inversion problem.

We will consider a system that evolves in an uncertain environment. The uncertainties appear, for example, due to manufacturing tolerances or environmental conditions. The numerical simulator modelling the system, denoted  $f$ , takes two types of input variables: a set of control variables  $\mathbf{x} \in \mathbb{X}$ , and a set of uncertain variables  $\mathbf{v} \in \mathcal{V}$ . Without any distributional assumptions for the uncertain variable  $\mathbf{v}$ , robust inversion (see Chevalier 2013) consists in seeking the set of control variables  $\mathbf{x} \in \mathbb{X}$  such that  $\sup_{\mathbf{v} \in \mathcal{V}} f(\mathbf{x}, \mathbf{v})$  is smaller than a threshold  $c$ . Then, the difficulty of solving the robust

---

✉ Mohamed Reda El Amri  
elamri.reda@yahoo.com

<sup>1</sup> IFP Energies Nouvelles, Rueil-Malmaison, France  
<sup>2</sup> Laboratoire Jean Kuntzmann, Université Grenoble Alpes, Grenoble, France  
<sup>3</sup> Université de Lyon, CNRS UMR 5208, Ecole Centrale de Lyon, Institut Camille Jordan, Villeurbanne, France  
<sup>4</sup> IFP Energies Nouvelles, Solaize, France

inversion problem strongly depends on the uncertainty set  $\mathcal{V}$ . In our setting,  $\mathcal{V}$  is a functional space, and we consider instead the inversion problem under uncertainty as a stochastic inversion problem, assuming that the uncertainty has a probabilistic description. Let  $V$  denote the associated random variable, valued in  $\mathcal{V}$ , modelling the uncertainty. In our framework, we are interested in recovering the set  $\Gamma^* := \{\mathbf{x} \in \mathbb{X}, g(\mathbf{x}) = \mathbb{E}_V[f(\mathbf{x}, V)] \leq c\}$ , with  $c \in \mathbb{R}$ . The functional random variable  $V$  is only known through a set of realizations, and the expectation has to be estimated. Moreover, the simulations are time-consuming, and thus, the usual Monte Carlo method to estimate the expectation ought to be avoided. Many reviews have been published to address this issue (see, e.g. L'Ecuyer and Lemieux 2005; L'Ecuyer and Owen 2009). Among the numerous techniques, the paper will focus on the ones based on the choice of a finite representative set of realizations of  $V$ , among the ones available. More precisely, these approaches aim at minimizing the expected distance between a random draw from the probability distribution of  $V$  and this finite set. In the case of vector-valued random variables, this type of methods, introduced in Flury (1990) as principal points, was employed in various statistical applications, including quantizer design (Luschgy and Pagès 2015; Pagès 2014) and stratified sampling. It is increasingly used for many engineering applications, where we are often faced with the challenge of working with *big data*. It is then necessary to reduce big data to manageable data. As for the case of functional random variables, various studies have been done in the Gaussian case (see Luschgy et al. 2010; Pagès and Printems 2005 and references therein). Here, we work in the special case where the functional variable  $V$  could be non-Gaussian and is only known through a finite sample of realizations. This paper proposes two new methodologies to perform this data reduction or quantization for functional random variable, and we investigate their performance in terms of integration errors.

Inversion problems have already been carried out in many applications, notably reliability engineering (see, e.g. Bect et al. 2012; Chevalier et al. 2014b), climatology (see, e.g. Bolin and Lindgren 2015; French and Sain 2013) and many other fields. In the literature, one way to solve the problem is to adopt a sequential sampling strategy based on Gaussian process emulators. The underlying idea is that Gaussian process emulators, which capture prior knowledge about the regularity of the unknown function  $g : \mathbf{x} \mapsto \mathbb{E}_V[f(\mathbf{x}, V)]$ , make it possible to assess the uncertainty about  $\Gamma^*$  given a set of evaluations of  $g$ . More specifically, these sequential strategies for the estimation of an excursion set are closely related to the field of Bayesian global optimization (see, e.g. Chevalier and Ginsbourger 2013). In the case of inversion problems, stepwise uncertainty reduction (SUR) strategies based on set measures were introduced in Vazquez and Bect (2009). More recently, a parallel implementation of these strategies has

been proposed in Chevalier et al. (2014b) and applied to the problem of recovery of an excursion set. Briefly, the strategy SUR gives sequentially the next location in the control space where to estimate the function  $g$  in order to minimize an uncertainty function. The key contribution of the present paper is to propose a data-driven adaptation of that procedure in the presence of functional uncertainties.

The paper is divided into five sections. Following this introduction, Sect. 2 is devoted to the introduction of two new adaptive methods to choose the finite representative set of the functional random variable for a reliable expectation estimation. In Sect. 3, we highlight the integration performance of our methods comparing to the standard Monte Carlo and to an existing method based on a probabilistic modelling with truncated principal component analysis (PCA). In Sect. 4, we introduce the Bayesian framework and fundamental notions for SUR infill strategies in the context of computationally costly simulations. In Sect. 5, we introduce the new proposed data-driven methodology for stochastic inversion under functional uncertainties and describe our algorithm. Finally, in Sect. 6, we illustrate the overall procedure on an analytical example and then apply it to an industrial test case.

## 2 Functional data reduction

In this section, we introduce new data reduction strategies for functional data in a greedy fashion. The first one is based on notion coming from functional quantization. The second one is related to notion of space-filling design. In this paper, data reduction aims at reducing the integration error when computing  $\mathbb{E}[f(\mathbf{x}, V)]$ . Therefore, we focus in Sect. 3 on the performance in terms of integration error of our strategies, comparing to standard procedures.

*Context* We consider the space  $\mathcal{H} = \mathbb{L}^2(\Omega, \mathcal{F}, \mathbb{P}; \mathcal{V})$  of random processes  $V$  with realizations  $V(\omega) = \mathbf{v}$  in the space of deterministic square-integrable functions defined on  $[0, T]$  denoted with  $\mathcal{V} = \mathbb{L}^2([0, T])$  and equipped with norm  $\|\mathbf{v}\| = (\int_0^T \mathbf{v}(t)^2 dt)^{1/2}$ . The random variables  $V(t, \cdot) = \eta$  lie in  $\mathbb{L}^2(\Omega)$ , the space of random variables with finite mean and variance, defined on  $(\Omega, \mathcal{F}, \mathbb{P})$  and equipped with norm  $\|\eta\|_{\mathbb{L}^2(\Omega)} = (\int_{\Omega} \eta^2 d\mathbb{P})^{1/2}$ . All random processes discussed in this paper lie in  $\mathcal{H}$  which is equipped with norm

$$\|V\|_{\mathbb{L}^2} = (\mathbb{E}[\|V\|^2])^{1/2} = \left( \mathbb{E} \left[ \int_0^T V(t)^2 dt \right] \right)^{1/2}, \tag{1}$$

for any  $V \in \mathcal{H}$ . The vast majority of realistic engineering problems can be addressed within this set of assumptions. We will consider a centred stochastic process with finite variance. We aim at summarizing the distribution of  $V$  through a finite collection of deterministic functions  $\{\mathbf{v}_j\}_{j=1}^l$  and corresponding weights  $\{w_j\}_{j=1}^l$ . Many reviews have been done

on *functional quantization* (Pagès and Printems 2005, 2009; Luschgy et al. 2010). For instance, Luschgy et al. (2010) propose different strategies for Gaussian processes.

An optimal quantization of  $V$  consists in finding the subset  $A \subset \mathcal{V}$  with  $\text{card}(A) \leq l$  that minimizes

$$\left( \mathbb{E} \left[ \min_{\mathbf{a} \in A} \|V - \mathbf{a}\|^2 \right] \right)^{1/2}. \tag{2}$$

Such a set is called an optimal  $l$ -quantizer. Lets us denote as  $A = \{\mathbf{a}_1, \dots, \mathbf{a}_l\}$ . We define a neighbour projection associated with  $A$  as:

$$\pi_A := \sum_{i=1}^l \mathbf{a}_i \mathbf{1}_{C_{\mathbf{a}_i}(A)}, \tag{3}$$

where  $\forall i \in \{1, \dots, l\}$   $C_{\mathbf{a}_i}(A)$  is the Voronoi partition induced by  $A$  and associated with  $\mathbf{a}_i$ :

$$C_{\mathbf{a}_i}(A) = \{ \mathbf{v} \in \mathcal{V} \mid \forall h \in \{1, \dots, l\}, \|\mathbf{v} - \mathbf{a}_i\| \leq \|\mathbf{v} - \mathbf{a}_h\| \}. \tag{4}$$

The  $A$ -quantization of  $V$  is defined by:

$$\hat{V}_l := \pi_A(V). \tag{5}$$

The projection  $\pi_A$  transforms  $V$  into its nearest neighbour in the set  $A$ . Voronoi partition is optimal in the sense that, for any random variable  $V'_l : \Omega \rightarrow A$ , one has  $\mathbb{E}\|V - V'_l\|^2 \geq \mathbb{E}\|V - \hat{V}_l\|^2$  (see, Pagès and Printems 2009). Finally, the  $l$ -quantization error of  $V$  is defined by

$$e_l(V) = \inf \{ (\mathbb{E}\|V - \hat{V}_l\|^2)^{1/2}, \hat{V}_l : \Omega \rightarrow \mathcal{V}, \text{card}(\hat{V}_l(\Omega)) \leq l \}. \tag{6}$$

From a computational point of view, the cost of minimizing the error defined in Eq. (6) is not negligible. Even in the finite-dimensional space  $\mathbb{R}^m$ , the numerical search of an optimal solution leads to an increasing computational cost when  $l$  or  $m$  grows (see Levrard 2014). Luschgy, Pagès propose in Luschgy and Pagès (2015) a greedy version of the  $\mathbb{L}^2$ -quantization problem for  $U$  an  $\mathbb{R}^m$  valued random vector. The greedy quantization is easier to compute in terms of complexity but provides a possible sub-optimal quantizer  $\{\hat{\mathbf{u}}_1, \dots, \hat{\mathbf{u}}_l\}$ . The authors in Luschgy and Pagès (2015) prove that the  $\mathbb{L}^2$ -quantization error at level  $l$  induced by  $\{\hat{\mathbf{u}}_1, \dots, \hat{\mathbf{u}}_l\}$  goes to 0 at rate  $l^{-1/m}$ . The idea of such a procedure is to determine sequentially the sequence  $(\hat{\mathbf{u}}_l)_{l \geq 1}$ . The first vector  $\hat{\mathbf{u}}_1$  achieves the error  $e_1(U)$ . Then, for  $l \geq 2$ ,

$$\forall l \geq 2, \hat{\mathbf{u}}_l \in \underset{\mathbf{u} \in \mathbb{R}^m}{\text{argmin}} (\mathbb{E}\|U - \hat{U}_l\|^2)^{1/2}, \tag{7}$$

where  $\hat{U}_l$  is the  $l$ -quantization induced by  $\{\hat{\mathbf{u}}_1, \dots, \hat{\mathbf{u}}_{l-1}\} \cup \{\mathbf{u}\}$ . In other words, the authors replace an optimization in dimension  $l \times m$  with  $l$  optimizations in dimension  $m$ .

In the present work, we propose a sequential strategy in a high-dimensional setting under the assumption that the random process  $V$  may not be Gaussian. In this framework, Miranda and Bocchini (2013, 2015) propose a one-shot algorithm that produces an optimal functional quantizer but which depends on a simulation procedure for  $V$ . In the following, we propose a greedy algorithm to compute a  $l$ -quantization of  $V$ . In our framework, the functional random variable is only known through a finite set of realizations. The specificity of our procedure is first that it does not require a simulation algorithm of the unknown process  $V$  (which is known only from a finite set of realizations), and secondly our quantizer can be sequentially increased in a greedy fashion. One ingredient in our methodology is the PCA decomposition of  $V$  (also known as Karhunen–Loève expansion).

Let us briefly recall the Karhunen–Loève expansion which is the most commonly employed method to reduce the statistical complexity of random fields indexed over bounded intervals, with continuous covariance function.

The Karhunen–Loève expansion Let  $V \in \mathcal{H}$  be a random process with zero mean and continuous covariance function  $C(t, s)$ . Then,

$$V(t) = \sum_{i=1}^{\infty} u_i \psi_i(t), \quad t \in [0, T], \tag{8}$$

where  $\{\psi_i\}_{i=1}^{\infty}$  are orthogonal and normalized eigenfunctions in  $\mathcal{V}$  of the integral operator corresponding to  $C$  :

$$\lambda_i \psi_i(t) = \int_0^T C(t, s) \psi_i(s) ds. \tag{9}$$

The  $\{u_i\}_{i=1}^{\infty}$  denotes a set of uncorrelated random variables with zero mean and variance  $\lambda_i$ , where  $\lambda_i$  is the eigenvalue corresponding to the eigenfunction  $\psi_i$ . In our method, we will truncate Eq. (8):

$$V(t) \simeq \sum_{i=1}^{m_{KL}} u_i \psi_i(t). \tag{10}$$

*Computational details for functional PCA* The covariance structure of the process  $V$  is unknown and has to be estimated from the data. More precisely,  $C(s, t)$  is estimated from the centred sample  $\mathcal{E} = \{\mathbf{v}_i\}_{i=1}^N$  by:

$$C^N(t, s) = \frac{1}{N} \sum_{i=1}^N \mathbf{v}_i(s) \mathbf{v}_i(t). \tag{11}$$

The eigenvalue problem defined by Eq. (9) is then solved by replacing  $C$  by  $C^N$  (see, e.g. Cardot et al. 1999 for convergence results). That approximated eigenvalue problem is solved, e.g. by discretizing the trajectories  $\{\mathbf{v}_i\}_{i=1,\dots,N}$  on  $[0, T] : \kappa = \{v_i(t_j)\}_{i=1,\dots,N}^{j=1,\dots,N_T}$ . It leads to the empirical covariance matrix defined as  $\hat{C}^N = \frac{1}{N}\kappa^T\kappa$ . We then have to solve a classical multivariate PCA with  $N_T$  variables given by a sample of size  $N$ . Standard PCA involves an  $O(\min(N_T^3, N^3))$  search for directions of maximum variance. In the case of discretized curves  $N_T \gg N$ , thus the complexity of PCA is  $O(N^3)$ .

Other approaches to implement functional PCA can be found in the literature. In Ramsay (2006), e.g. the authors propose to expand the curves as linear combinations of spline basis functions, and to apply PCA to the coefficients of the curves on the spline basis. There are several criteria for the choice of the truncation argument  $m_{KL}$  (Jackson 1993). One can cite the Kaiser-Guttman criterion which consists of choosing the first components with eigenvalues higher than 1. Instead of using the absolute value of the explained variance, as indicated by the eigenvalue, the choice of  $m_{KL}$  could be based on the “percentage of variance” given by the proportion  $\frac{\lambda_i}{\sum_{i=1}^N \lambda_i}$ . By this way, we choose  $m_{KL}$  so that the percentage of variance explained by the first components exceeds a certain threshold. Often to avoid the arbitrary choice of the threshold, we display the eigenvalues in a downward curve and extract the components on the steep slope.

What is important to note is that functional PCA is done once for all, as an offline pre-processing step in our global inversion procedure.

$\mathbb{L}^2$ -Greedy functional quantization ( $\mathbb{L}^2$ -GFQ) Now, we aim at optimally exploring the range of variations of  $V$  with a few elements in  $\mathcal{E}$ . Let  $\mathcal{G} = \{(\langle \mathbf{v}, \psi_1 \rangle, \dots, \langle \mathbf{v}, \psi_{m_{KL}} \rangle)\}^T, \mathbf{v} \in \mathcal{E} = \{\mathbf{u}_i\}_{i=1}^N$ , with  $\mathbf{u}_i = (\langle \mathbf{v}_i, \psi_1 \rangle, \dots, \langle \mathbf{v}_i, \psi_{m_{KL}} \rangle)^T$ , be the set of the first  $m_{KL}$  coefficients in KL expansion (see Fig. 1). Since we place ourselves in a finite space  $\mathcal{G} \subset \mathbb{R}^{m_{KL}}$ , a first step consists in an efficient and sequential strategy for the selection of a vectorial  $l$ -quantizer. A first solution is to apply the greedy vectorial quantization procedure described by Eq. (7). Let  $U$  be a random vector with discrete uniform distribution on  $\mathcal{G}$ . The sequential construction is detailed as follows

$$\begin{aligned} \hat{D}_1 &= \{\hat{\mathbf{u}}_1\} \text{ where } \hat{\mathbf{u}}_1 \text{ is a solution of } e_1(U) \text{ from Eq. (6)} \\ \forall l \geq 2, \hat{D}_l &= \hat{D}_{l-1} \cup \{\hat{\mathbf{u}}_l\} \\ \text{where } \hat{\mathbf{u}}_l &\in \arg \min_{\mathbf{u} \in \mathcal{G}} (\mathbb{E} \|\mathbf{U} - \mathbf{U}_l\|^2)^{1/2}, \\ l &= l + 1, \\ \text{and } \mathbf{U}_l &\text{ is the } l\text{-quantization induced by } \{\hat{\mathbf{u}}_1, \dots, \hat{\mathbf{u}}_{l-1}\} \\ &\cup \{\mathbf{u}\}. \end{aligned} \tag{12}$$

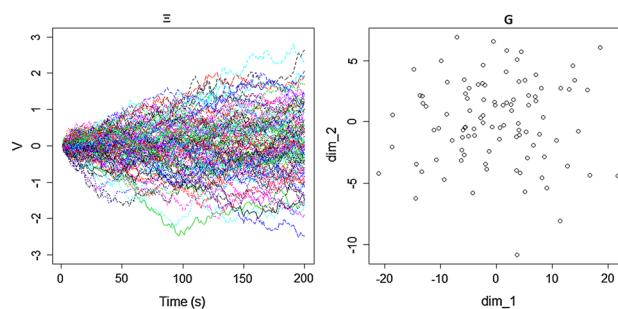


Fig. 1  $\mathcal{E}$  is a sample of 100 realizations of  $V$  (left) and  $\mathcal{G}$  the corresponding representation in the truncated space of coefficients with  $m_{KL} = 2$  (right)

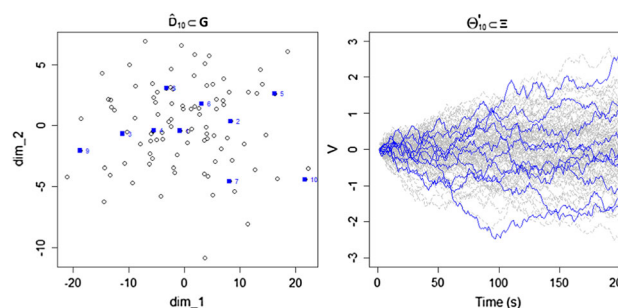


Fig. 2 Sequential design of ten points (bold points) in the set of the coefficients  $\mathcal{G}$  (left) and their corresponding bold curves in  $\mathcal{E}$  (right)

A collection of representative curves associated with our functional random variable  $V$  is obtained by recovering the curves in the initial sample  $\mathcal{E}$  that correspond to the selected points  $\hat{D}_l$ :

$$\hat{D}_l = \{\hat{\mathbf{u}}_i\}_{i=1}^l \subset \mathcal{G} \longrightarrow \Theta'_l = \{\theta'_i\}_{i=1}^l \subset \mathcal{E} \tag{13}$$

This step is important as it allows recovering the functional variability of  $V$  and not only the variability of its first  $m_{KL}$  coefficients. Figure 2 shows the algorithm up to step  $l = 10$  on the example of Fig. 1. Note that, from this figure, we can see that  $\mathbb{L}^2$ -quantization leads to selecting central points and so the sample  $\Theta'_{l=10}$  is mainly representative of the mean behaviour of  $V$ . We also note that the extreme points are not chosen in the beginning of the construction. To address this issue, we propose a method that aims at exploring the range of variations of  $V$  by selecting central points and also extreme points. One way to do so consists in the construction of a space-filling design in  $\mathbb{R}^{m_{KL}}$ . Let  $\tilde{D}$  be this design. As the distribution of  $V$  is only known through  $\mathcal{E}$ , it is natural to search  $\tilde{D}$  included in  $\mathcal{G}$  such that the chosen points are well spread all over the space. Let us recall the notion of space-filling design, from a purely model-free stance.

*Space-filling design and criterion* Let us define  $D = \{\mathbf{u}_1, \dots, \mathbf{u}_l\}$  a collection of  $l$  points. We denote by  $\text{dist}_{ij} = \|\mathbf{u}_i - \mathbf{u}_j\|$  the euclidean distance between two design points

$\mathbf{u}_i$  and  $\mathbf{u}_j$  of  $D$ . One must then attempt to make the smallest distance between neighbouring points in  $D$  as large as possible. We call a design that maximizes  $\phi_{Mm}(D) = \min_{i \neq j} \text{dist}_{ij}$ , a **maximin-distance design** (see Johnson et al. 1990). There are several other intrinsic criteria in the literature such as discrepancy that measures whether the distribution of the points of  $D$  is close to a uniform distribution. See Pronzato and Müller (2012) for a detailed overview on the subject. In the following, we consider the maximin-distance criterion to construct our design, and since we want to select points from the set of coefficients  $\mathcal{G}$ , the design  $\tilde{D}$  can be obtained by finding the design of  $l$  points among  $N$ , which maximizes the criterion  $\phi_{Mm}$ .

*Maximin-Greedyfunctional quantization (Maximin-GFQ)*  
 Finding the design  $\tilde{D}$  is a computationally difficult task. We could adapt one of the optimal design algorithms used in the literature such as simulated annealing (see Morris and Mitchell 1995) and stochastic evolutionary algorithm (see Jin et al. 2005) for our purpose. Here, we propose a one-point-at-time greedy algorithm for the generation of our design. The sequential construction is described as follows

Initialization:  $\tilde{D}_1 = \{\tilde{\mathbf{u}}_1\}$  where  $\tilde{\mathbf{u}}_1$  is randomly chosen

$$\forall l \geq 2, \tilde{D}_l = \tilde{D}_{l-1} \cup \{\tilde{\mathbf{u}}_l\}$$

where  $\tilde{\mathbf{u}}_l \in \arg \max_{\mathbf{u} \in \mathcal{G}} \phi_{Mm}(\tilde{D}_{l-1} \cup \{\mathbf{u}\})$ ,

$$l = l + 1. \tag{14}$$

The algorithm starts with a random point  $\tilde{\mathbf{u}}_1$ , and the next point is chosen among the points in  $\mathcal{G}$  in order to maximize the maximin-distance criterion. Besides the sequentiality as for the  $\mathbb{L}^2$ -GFQ method, the points are now chosen in order to explore the range of variations of  $V$  at each step using a distance criterion. Meaning that at each step, the exploration of the domain is reasonable. The technique to recover the curves remains the same:

$$\tilde{D}_l = \{\tilde{\mathbf{u}}_i\}_{i=1}^l \subset \mathcal{G} \longrightarrow \Theta_l'' = \{\theta_i''\}_{i=1}^l \subset \mathcal{E} \tag{15}$$

In order to make a comparison, we start the Maximin-GFQ method Eq. (15) with the same point as the  $\mathbb{L}^2$ -GFQ method Eq. (13), i.e.  $\tilde{\mathbf{u}}_1 = \hat{\mathbf{u}}_1$ . Figure 3 shows the results up to step  $l = 10$  of both procedures. One can observe that the greedy maximin method covers well the range of variation of  $V$  contrary to the  $\mathbb{L}^2$ -GFQ method, which provides spread points only on the first component. The  $\mathbb{L}^2$ -GFQ seems to be more influenced by the higher-order KL expansion. In the following, in order to improve the readability, we adopt the simplified notation  $\Theta_l$  that refers to one of the two constructions  $\Theta_l''$  and  $\Theta_l'$ . In this way and in the same spirit as

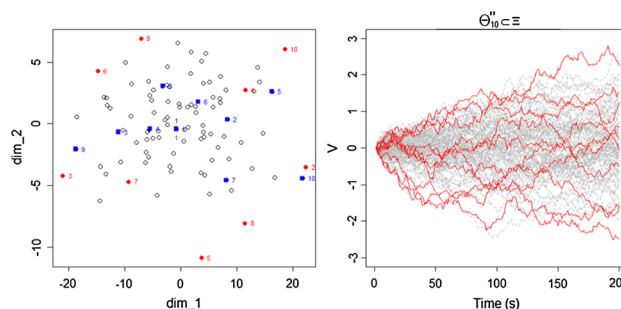


**Fig. 3** Left: two designs of  $l = 10$  points in the 2D-coefficients set  $\mathcal{G}$ . Maximin-GFQ (red circle points) and greedy  $\mathbb{L}^2$ -GFQ (blue square points). Right: the corresponding red curves for the Maximin-GFQ procedure (right). (Colour figure online)

before [see Eqs. (3), (5)], we define  $\Theta_l$ -quantization of the stochastic process  $V$  as

$$\hat{V}_l = \sum_{i=1}^l \theta_i \mathbf{1}_{C_{\theta_i}}(V), \tag{16}$$

where  $\{C_{\theta_i}(\Theta_l) : \theta_i \in \Theta_l\}$  is a Voronoi partition of  $\mathcal{E}$  induced by  $\Theta_l$  as defined in Eq. (4).

Regarding the computational time devoted to perform the functional quantization, Fig. 4 shows the time needed to compute the whole Greedy Functional Quantization as a function of point set size  $l$ . The KL expansion is done in a prior unaccounted step that takes 0.11 s. These algorithms are implemented in the software R, and all computations are performed on a 2.80GHz processor. From this figure, the running time of the maximin-GFQ method grows much more slowly than the  $\mathbb{L}^2$ -GFQ one. Indeed, the discrete optimization in the  $\mathbb{L}^2$ -GFQ method [Eq. (12)] involves an empirical estimation of the expectation at each step; thus, the algorithm has complexity  $O(N^2 \times l \times m_{KL})$ . The latter becomes time-consuming as  $l$  increases comparing to the maximin-GFQ algorithm which has complexity  $O(N \times l \times m_{KL})$ .

The reasons for performing a dimension reduction are twofold. The first one is computational as illustrated in Fig. 4, where both methods are compared to the  $\mathbb{L}^2$ -GFQ without KL decomposition with complexity  $O(N^2 \times l \times N_T)$ . The second one is related to the properties of the maximin criterion. Indeed, the space-filling quality is higher in a small dimensional space since in a high one too many points are chosen at the boundary (see e.g. Abtini 2018; Pronzato and Müller 2012).

We recall that this functional PCA step is done once for all in a pre-processing step.

In this section, we have introduced two data-driven greedy original procedures for functional quantization, quantization being an alternative to Monte Carlo methods for numerical integration. In the next section, we highlight the performance of these procedures through two analytical examples.

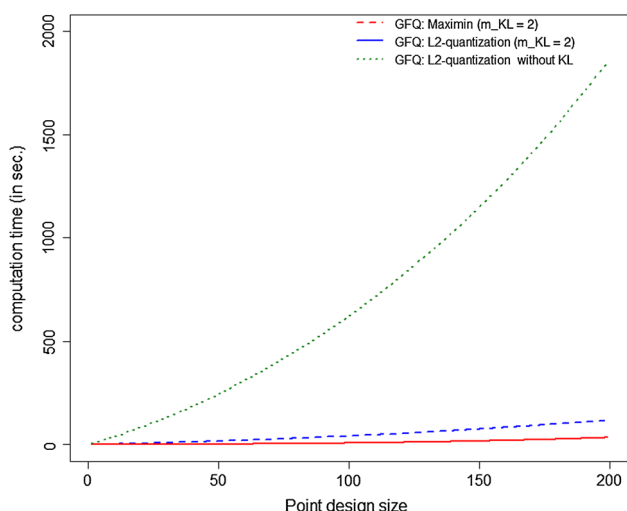


**Fig. 4** Computation time (in seconds) of the GFQ methods as a function of point set size ( $N = 200, N_T = 200$ )

### 3 Numerical integration

Let  $h : \mathcal{V} = \mathbb{L}^2([0, T]) \rightarrow \mathbb{R}$  be a continuous function, and let  $\hat{V}_l$  be a  $l$ -quantization. It is natural to approximate  $\mathbb{E}[h(\mathbf{V})]$  by  $\mathbb{E}[h(\hat{V}_l)]$ . This quantity  $\mathbb{E}[h(\hat{V}_l)]$  is simply the finite weighted sum:

$$\mathbb{E}[h(\hat{V}_l)] = \sum_{i=1}^l h(\theta_i) \mathbb{P}(\hat{V}_l = \theta_i), \tag{17}$$

where the distribution  $(\mathbb{P}(\hat{V}_l = \theta_i))_{i=1:l}$  of  $\hat{V}_l$  can be approximated empirically by  $(\text{card}(C_{\theta_i}(\Theta_l) \cap \mathcal{E}) / \text{card}(\mathcal{E}))_{i=1:l}$ . For a given  $i$ , this is the proportion of curves among  $N$  which are closer to  $\theta_i$  than to any other  $\theta_j, j \neq i$ . This proportion acts as a weight in the computation of the expectation. Assigning weights can bring a significant improvement (see L'Ecuyer and Lemieux 2005).

**Remark** Under regularity assumptions, the integration error can be bounded by the quantization error. For example, if  $h$  is Lipschitz in the sense that  $\forall \mathbf{v}, \mathbf{v}' \in \mathcal{V}, |h(\mathbf{v}) - h(\mathbf{v}')| \leq c\|\mathbf{v} - \mathbf{v}'\|$ , then

$$\begin{aligned} |\mathbb{E}[h(\mathbf{V})] - \mathbb{E}[h(\hat{V}_l)]| &\leq \mathbb{E}|h(\mathbf{V}) - h(\hat{V}_l)| \\ &\leq c\mathbb{E}\|\mathbf{V} - \hat{V}_l\| \\ &\leq c(\mathbb{E}\|\mathbf{V} - \hat{V}_l\|^2)^{1/2}. \end{aligned} \tag{18}$$

Returning to our original notation  $\mathbb{E}[f(\mathbf{x}, \mathbf{V})]$ , the proposed methodologies for an efficient estimation of the expectation over a functional random variable are summarized in Algorithms 1 and 2.

#### Algorithm 1 maximin-GFQ: Numerical integration

- 1: **Inputs:** initial sample ( $\mathcal{E}$ ), truncation argument ( $m_{KL}$ ),  $\mathbf{x}$  value where the expectation will be evaluated and set size of the quantization ( $l$ ).
- 2:  $\mathcal{G} \leftarrow$  truncation of the KL expansion after  $m_{KL}$ -terms.
- 3: Construct the set of representative points  $\tilde{D}_l$  defined by Eq. (14).
- 4: Induce from  $\tilde{D}_l$  the corresponding set of representative curves  $\Theta_l''$  Eq. (15).
- 5: Define  $\hat{V}_l \leftarrow \Theta_l''$ -quantization of  $\mathbf{V}$  Eq. (16).
- 6: Perform the computation of the expectation  $\mathbb{E}[f(\mathbf{x}, \hat{V}_l)]$  Eq. (17):
- 7:  $\mathbb{E}[f(\mathbf{x}, \mathbf{V})] \approx \mathbb{E}[f(\mathbf{x}, \hat{V}_l)] = \sum_{i=1}^l f(\mathbf{x}, \theta_i'') \mathbb{P}(\hat{V}_l = \theta_i'')$ .

#### Algorithm 2 $\mathbb{L}^2$ -GFQ: Numerical integration

- 1: **Inputs:** initial sample ( $\mathcal{E}$ ), truncation argument ( $m_{KL}$ ),  $\mathbf{x}$  value where the expectation will be evaluated and set size of the quantization ( $l$ ).
- 2:  $\mathcal{G} \leftarrow$  truncation of the KL expansion after  $m_{KL}$ -terms.
- 3: Construct the set of representative points  $\hat{D}_l$  defined by Eq. (12).
- 4: Induce from  $\hat{D}_l$  the corresponding set of representative curves  $\Theta_l'$  Eq. (13).
- 5: Define  $\hat{V}_l \leftarrow \Theta_l'$ -quantization of  $\mathbf{V}$  Eq. (16).
- 6: Perform the computation of the expectation  $\mathbb{E}[f(\mathbf{x}, \hat{V}_l)]$  Eq. (17):
- 7:  $\mathbb{E}[f(\mathbf{x}, \mathbf{V})] \approx \mathbb{E}[f(\mathbf{x}, \hat{V}_l)] = \sum_{i=1}^l f(\mathbf{x}, \theta_i') \mathbb{P}(\hat{V}_l = \theta_i')$ .

In the sequel, we compare these two algorithms to the standard Monte Carlo, whose steps are outlined in Algorithm 3. The estimation of the expectation is sequentially calculated in the same vein as the GFQ procedures.

#### Algorithm 3 Crude MC: Numerical integration

- 1: **Inputs:** initial sample ( $\mathcal{E}$ ),  $\mathbf{x}$  value where the expectation will be evaluated and set size of the quantization ( $l$ ).
- 2: Sample  $\bar{V}_l = \{\bar{v}_i\}_{i=1}^l$  where  $\bar{v}_1, \dots, \bar{v}_l \stackrel{i.i.d.}{\sim} \mathbb{U}_{\mathcal{E}}$ , where  $\mathbb{U}_{\mathcal{E}}$  a discrete uniform distribution on  $\mathcal{E}$ .
- 3: Estimate the expectation  $\mathbb{E}[f(\mathbf{x}, \mathbf{V})]$  by  $l$  MC runs to  $f(\mathbf{x}, \bar{v})$ :
- 4:  $\mathbb{E}[f(\mathbf{x}, \mathbf{V})] \approx \frac{1}{l} \sum_{i=1}^l f(\mathbf{x}, \bar{v}_i)$ .

We consider two analytical examples to highlight the integration performances of the two Greedy Functional Quantization methods (GFQ) in comparison with crude Monte Carlo. The first example is defined as an additive Lipschitz function, i.e. sum of the 2D Bohachevsky function and uncertainties. The second example does not verify the Lipschitz assumptions to mimic real applications.

*Application 1* We consider a functional  $f$  defined as

$$\begin{aligned} f : \mathbf{v} \mapsto & (a^2 + 2b^2 - 0.3 \cos(3\pi a) \\ & - 0.4 \cos(4\pi b) + 0.7) + \int_T e^{\mathbf{v}^t} dt, \end{aligned}$$

where  $a = 50, b = -80$  and  $\mathbf{V}$  is a standard Brownian motion on  $\mathbb{R}$  and  $[0, T] = [0, 1]$ . We suppose that a sample

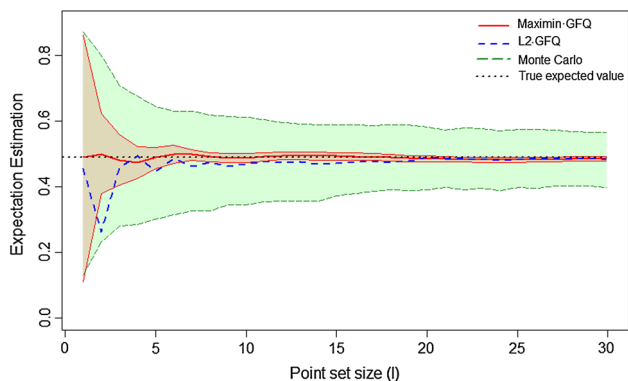


**Fig. 5** Application 1. Sequential expectation estimation ( $m_{KL} = 2$ ). Lines denote the average estimates, and coloured bands mark the 25th and 75th quantiles (Monte Carlo (in green) and maximin-GFQ (in red)). Horizontal axis denotes the number of curves  $l$  used for the expectation estimation. (Colour figure online)

$\mathcal{E}$  of  $N = 200$  realizations of  $V$  is available and that the probability distribution of  $V$  is unknown. These realizations are discretized on a regular grid of  $N_T = 200$  points. In this example, we fix the truncation argument at 2 to explain 90% of the variance. Because of the random choice of the starting curve, the maximin-GFQ methods have a stochastic behaviour like the Monte Carlo method. To account for these variabilities in the test, the performance is averaged over 200 independent runs for the MC method and 200 runs related to all the different starting curves for the maximin-GFQ method.

The results are shown in Fig. 5. We observe that for any choice of  $l$ , the integration error induced by any of both GFQ methods is significantly smaller than the standard Monte Carlo. One can note that the maximin-GFQ method is less sensitive to the starting point from set size  $l \geq 25$ . We also remark that for a small size  $l \leq 5$ , the maximin-GFQ method is not yet stabilized implying more uncertainties in the estimation. From  $l \geq 10$  (see Fig. 3), stability is reached thanks to the procedure of selection of different kinds of curves (centred and extreme).

*Application 2* We define a function  $f$  by mixing control variables and uncertainties. This function involves  $\max(\mathbf{v})$  and  $\min(\mathbf{v})$ , so catching the variability of  $V$  becomes important. The function  $f$  is given by

$$f : \mathbf{v} \mapsto \max_t \mathbf{v}_t \cdot |0.1 \cos(a \max_t \mathbf{v}_t) \sin(b) \cdot (a + b \min_t \mathbf{v}_t)^2| \cdot \int_0^T (30 + \mathbf{v}_t)^{\frac{a \cdot b}{20}} dt,$$

where  $a = 2.95$ ,  $b = 3.97$  and  $V$  is a standard Brownian motion on  $\mathbb{R}$  and  $[0, T] = [0, 1]$ . To mimic real applications, we assume in the procedure that the probability distribution of  $V$  is unknown. We suppose that a sample  $\mathcal{E}$  of  $N = 200$  realizations of  $V$  is available. These realizations are discretized on a grid of size  $N_T = 200$ . We note that the two

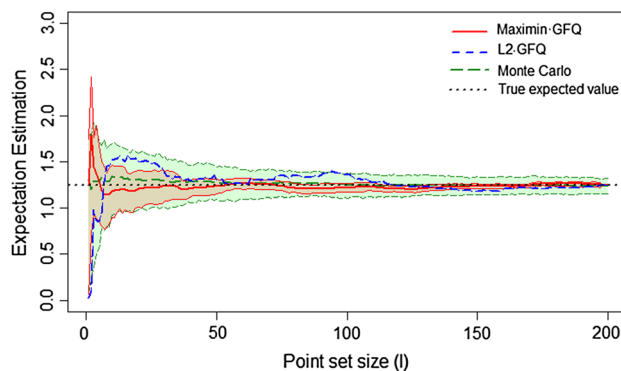


**Fig. 6** Application 2. Sequential expectation estimation ( $m_{KL} = 2$ ). Lines denote the average estimates, and coloured bands mark the 25th and 75th quantiles [Monte Carlo (in green) and maximin-GFQ (in red)]. Horizontal axis denotes the number of curves  $l$  used for the expectation estimation. (Colour figure online)

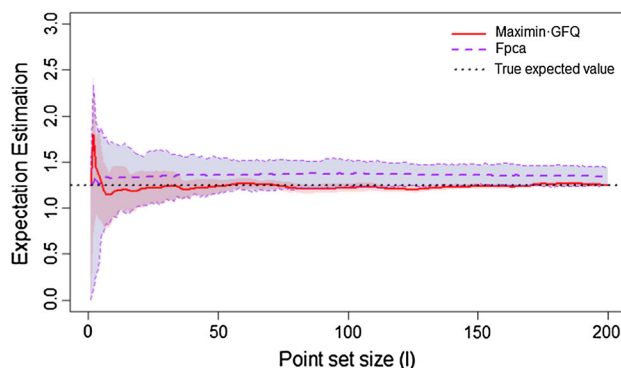


**Fig. 7** Application 2. Sequential expectation estimation ( $m_{KL} = 2$ ). Lines denote the average estimates, and coloured bands mark the 25th and 75th quantiles [FPCA (in blue) and maximin-GFQ (in red)]. Horizontal axis denotes the number of curves  $l$  used for the expectation estimation. (Colour figure online)

GFQ methods depend on the truncation argument  $m_{KL}$ . In this example, we fix it at 2 to explain 90% of the variance. (Results are similar for other truncation arguments and  $\mathbf{x}$  values, and are omitted for brevity.)

Due to the stochastic nature of the Monte Carlo and the maximin-GFQ methods, the performance of the method is averaged over 200 independent runs for the MC method and 200 runs related to different starting curves for the maximin-GFQ method. The results of the integration algorithms are shown in Fig. 6. The lines indicate average estimate, and the coloured bands mark the area between the 25th and 75th quantiles. Here, two observations can be made. First, for any choice of  $l$ , the integration error induced by both GFQ methods is significantly smaller than the standard Monte Carlo. Secondly, for maximin-GFQ method, the variability induced by the choice of the starting point is weak from set size  $l \geq 20$ .

We recall that our procedure is based on a dimension reduction. However, once the space-filling design has been

built in  $\mathbb{R}^{m_{KL}}$ , we go back to the high-dimensional space  $\mathcal{V}$  by selecting the corresponding curves. We expect such a procedure to be robust to the dimension reduction. To illustrate this intuition, we compare the maximin-GFQ algorithm to an existing method, called hereafter FPCA method. This latter consists in sampling independently the KL random variables  $U \in \mathbb{R}^{m_{KL}}$  whose probability distribution is estimated beforehand and denoted  $\mathbb{P}_U$  [see, e.g. Nanty et al. (2016) for a detailed overview on the subject]. Then, we obtain the desired curves using the linear combination of Eq. (10). The results of the comparison are shown in Fig. 7. We note that the FPCA method leads to a biased estimation due to the regularization induced by reducing the dimension.

In summary, these simulations show that the two GFQ methods benefit improved performances over Monte Carlo in numerical accuracy.

In this section, we presented a methodology to efficiently estimate the expectation over  $V$  at a point  $\mathbf{x}$  in the control space  $\mathbb{X}$ . In the next section, we recall an existing method to address the inversion problem in the control variable space in the context of computationally costly simulations. This strategy is defined within a Bayesian framework and based on the so-called stepwise uncertainty reduction strategy (SUR). Let us start with some presentation of SUR paradigm.

### 4 Background on SUR strategies

Let  $f : \mathbb{X} \times \mathcal{V} \rightarrow \mathbb{R}$  denote a real-valued continuous function, where  $\mathbb{X}$  is a bounded subset of  $\mathbb{R}^p$ ,  $p \geq 1$ , and  $\mathcal{V}$  a functional space on which a random variable  $V$  is defined. Moreover, we suppose that a finite set of  $N$  independent and identically distributed realizations of the functional random variable  $V$  is available. In the following, we consider the expectation over the distribution of the functional random variable and we are interested in characterizing the set of control variables which leads to the safe behaviour of a system:

$$\begin{aligned} \Gamma^* &=: \{ \mathbf{x} \in \mathbb{X}, \mathbb{E}_V[f(\mathbf{x}, V)] \in C \} \\ &= \{ \mathbf{x} \in \mathbb{X}, g(\mathbf{x}) \in C \} \text{ with } C = (\infty, c], c \in \mathbb{R}. \end{aligned} \tag{19}$$

While the function  $f$  depends on two separate types of inputs (control and uncertain variables), our objective function  $g$  depends only on the control variables, i.e. for each setting of control variables, the objective function is the mean of  $f$  over the unknown distribution of the uncertain variable.

The estimation of  $\Gamma^*$  by evaluating the function  $g$  at each grid point of the discretized version of  $\mathbb{X}$  requires far too many evaluations of  $g$ . Therefore, statistical methods based on a reduced number of evaluation points are widely used to overcome this latter difficulty by focusing the evaluations on the 'promising' subregion of the control space.

These methods usually begin by an exploration phase, during which the output of the code is computed on an experimental design of size  $n$ . This initial design is then sequentially expanded by adding new goal-oriented points. These sequential strategies have been used in recent years for many purposes, such as the failure probability estimation (Bect et al. 2012) and target regions (Picheny et al. 2010) whose main idea is to decrease the kriging variance at the points where the kriging mean is close to the threshold  $c$ . Unlike the two aforementioned methods, we are interested in the whole excursion set. In Chevalier et al. (2013, 2014a), the sampling criterion is based on the concept of random closed sets and applied to identify the set  $\Gamma^*$ . In this work, we adopt this strategy and the procedure is introduced as follows.

#### 4.1 Random closed set and Bayesian framework

In a Bayesian framework, we assume that  $g$  is a realization of an almost surely continuous Gaussian process  $Y \sim GP(m, k)$  with a mean structure  $m$ , defined as,  $m(\mathbf{x}) = \mathbb{E}[Y_{\mathbf{x}}]$ ,  $\mathbf{x} \in \mathbb{X}$ , and a covariance kernel  $k$ , defined as,  $k(\mathbf{x}, \mathbf{x}') := Cov(Y_{\mathbf{x}}, Y_{\mathbf{x}'})$ ,  $\mathbf{x}, \mathbf{x}' \in \mathbb{X}$ . Due to the stochastic nature of  $(Y_{\mathbf{x}})_{\mathbf{x} \in \mathbb{X}}$ , the associated excursion set,

$$\Gamma := \{ \mathbf{x} \in \mathbb{X}, Y_{\mathbf{x}} \in C \} \tag{20}$$

is a random closed set. From the assumption that  $g$  is a realization of  $Y$ , the true unknown set  $\Gamma^*$  can be seen as a realization of the random closed set  $\Gamma$ . It is possible to compute a mean and deviation for this random set  $\Gamma$  by the Vorob'ev approach (see Chevalier et al. 2013). We use the Vorob'ev expectation  $Q_{\alpha^*}$  as an estimator of the true excursion set and Vorob'ev deviation  $\mathbb{E}[\mu(\Gamma \Delta Q_{\alpha^*})]$  to quantify the uncertainty of the random closed set  $\Gamma$ . Therefore, we implement a Stepwise Uncertainty Reduction strategy (SUR) that aims at reducing uncertainty on  $\Gamma$  by adding new evaluation points step by step as proposed by Chevalier et al. (2013). The principle of SUR strategies is also recalled in Sect. 4.2.

#### 4.2 SUR strategies

The principle of stepwise uncertainty reduction (SUR) (see, e.g. Bect et al. 2012; Chevalier et al. 2014b) is to define an uncertainty measure, depending on the objective to be fulfilled, and to sequentially choose the points that decrease most this uncertainty. In other words, the aim of the SUR strategy is to construct a sequence of evaluation locations in order to reduce the *expected* uncertainty on a quantity of interest.

Here, we work in the setting where  $g$  is a sample path of a random process  $Y$ . The uncertainty function for an estimate of  $\Gamma$  is defined as a function  $\mathcal{H}^{\text{uncert}}$  that associates with any finite sequence of observations  $(\mathcal{X}_n, \mathbf{g}_{\mathcal{X}_n})$  a real value

representing the uncertainty on the estimation of  $\Gamma$ . When  $n$  observations are available, we denote by  $\mathcal{H}_n^{\text{uncert}}$  the uncertainty at step  $n$ . We assume that we have  $r$  evaluations left. The objective of the SUR strategy is to find  $r$  optimal locations  $\mathbf{x}_{n+1}, \dots, \mathbf{x}_{n+r}$  such that the uncertainty  $\mathcal{H}_{n+r}^{\text{uncert}}$  is as small as possible.

In what follows, we consider the Vorob'ev deviation as the uncertainty function, at step  $n$ ,

$$\mathcal{H}_n^{\text{uncert}} = \mathbb{E}[\mu(\Gamma \Delta Q_{n, \alpha_n^*}) \mid Y_{\mathcal{X}_n} = \mathbf{g}_{\mathcal{X}_n}], \tag{21}$$

where  $Q_{n, \alpha_n^*}$  is the Vorob'ev expectation conditionally to the  $n$  available observations. One way of constructing the sequence  $\mathbf{x}_{n+1}, \dots, \mathbf{x}_{n+r}$  is to choose at each step the point that gives the smallest uncertainty  $\mathcal{H}_{n+1}^{\text{uncert}}$ ,

$$\mathcal{H}_{n+1}^{\text{uncert}}(\mathbf{x}) = \mathbb{E}[\mu(\Gamma \Delta Q_{n+1, \alpha_{n+1}^*}) \mid Y_{\mathcal{X}_n} = \mathbf{g}_{\mathcal{X}_n}, Y_{\mathbf{x}}] \tag{22}$$

We note that the future uncertainty  $\mathcal{H}_{n+1}^{\text{uncert}}$  is function of  $Y_{\mathbf{x}}$  given  $Y_{\mathcal{X}_n} = \mathbf{g}_{\mathcal{X}_n}$ . Therefore, at each step we choose the point that gives the smallest uncertainty in expectation, that is :

$$\begin{aligned} \mathbf{x}_{n+1} &\in \underset{\mathbf{x} \in \mathbb{X}}{\text{argmin}} \mathbb{E}_{n, \mathbf{x}}[\mathcal{H}_{n+1}^{\text{uncert}}(\mathbf{x})] \\ &:= \underset{\mathbf{x} \in \mathbb{X}}{\text{argmin}} \mathcal{J}_n(\mathbf{x}), \end{aligned} \tag{23}$$

where  $\mathbb{E}_{n, \mathbf{x}}$  denotes the expectation with respect to  $Y_{\mathbf{x}} \mid Y_{\mathcal{X}_n} = \mathbf{g}_{\mathcal{X}_n}$  [for detailed formula of  $\mathcal{J}_n(\cdot)$ , see Chevalier et al. (2013)].

After having evaluated the function  $g$  at the optimal location  $\mathbf{x}_{n+1}$ , we update the parameters of the posterior mean and covariance, and we restart until the evaluation budget  $r$  is spent. Such strategy is called *one-step lookahead*, which means that we select the next evaluation point as if it were the last one. A comparison of such a strategy to the space-filling strategy based on Sobol sequences is given in Chevalier et al. (2013). The authors highlight the effectiveness of the SUR strategy through an analytical example. For more theoretical perspectives on the SUR strategies, see Bect et al. (2016) and references therein.

### 4.3 SUR strategy adapted to noisy observations

In our context, we cannot compute exact evaluations of the expectation over the probability distribution of  $V$ . We propose in Sect. 2 sequential algorithms that efficiently approximate the value of  $g(\mathbf{x})$  by  $\mathbb{E}[f(\mathbf{x}, \hat{V}_i)]$ . On the design points, the  $n$  evaluations  $\mathbf{g}(\mathcal{X}_n)$  are replaced by their approximation  $\tilde{\mathbf{g}}(\mathcal{X}_n) = (\mathbb{E}[f(\mathbf{x}_1, \hat{V}_1)], \dots, \mathbb{E}[f(\mathbf{x}_n, \hat{V}_n)])$ . For that reason, we do not want to build an exact interpolant at points  $\mathbf{x}_1, \dots, \mathbf{x}_n$ . We rather consider that  $\tilde{\mathbf{g}}(\mathcal{X}_n)$  are realizations of a Gaussian vector  $(\tilde{Y}_{\mathbf{x}_1}, \dots, \tilde{Y}_{\mathbf{x}_n})^T$  defined by  $\tilde{Y}_{\mathbf{x}_i} := Y_{\mathbf{x}_i} + \varepsilon_i$ ,

where  $\varepsilon_1, \dots, \varepsilon_n$  are independent centred Gaussian variables of variance  $\tau_1^2, \dots, \tau_n^2$ . Conditionally to  $\tilde{Y}_{\mathbf{x}_1}, \dots, \tilde{Y}_{\mathbf{x}_n}$ , the process  $Y$  is still Gaussian except that we add the variances  $\{\tau_i^2\}_{i=1}^n$  to the diagonal elements of the covariance matrix.

**Remark** In our context, we estimate the expectation empirically by  $l$  calls to the function  $f$ . The well-known Monte Carlo methods (Crude MC, FPCA) allow us to quantify the noise of estimation and to integrate it into GP modelling (kriging with noisy observations). Consequently, we define the variance components  $\{\tau_i^2\}_{i=1}^n$  as the sample variance estimators  $\tau_i^2 = \text{var}(f(\mathbf{x}_i, \tilde{V}_i))$  for the crude MC method and  $\text{var}(f(\mathbf{x}_i, V_i^{\text{pca}}))$  for the FPCA method.

## 5 Algorithm coupling SUR and functional quantization

The whole computational aspect is carried out in the **R** environment: we use the `DiceKriging` package (Roustant et al. 2013) for Gaussian modelling, and the sampling criterion  $\mathcal{J}_n$  Eq. (23), used in order to select the next evaluation  $\mathbf{x}_{n+1}$  of the function  $g$ , is already implemented in the `KrigInv` package (Chevalier et al. 2014a). We exploit the kriging update formulas (Chevalier et al. 2015) for faster updates of posterior mean and covariance. When  $\mathbf{x}_{n+1}$  is identified,  $l$  calls to the simulator have to be performed to approximate the expectation on that point. The sequentiality of our estimation method of the expectation on  $\mathbf{x}_{n+1}$  leads us to define a *stopping criterion* on the expectation estimation  $\hat{m}$ . Thus,  $l$  is chosen sufficiently large so that  $l_0$  consecutive 'expectation variations' are smaller than a threshold  $\varepsilon$ . Besides, the number of calls  $l$  will naturally depend on  $\mathbf{x}_{n+1}$ .

In practice, at each step of the estimation we evaluate the absolute difference between two consecutive estimations of the expectation,

$$e_l(\mathbf{x}_{n+1}) = |\hat{m}_{l-1}(\mathbf{x}_{n+1}) - \hat{m}_l(\mathbf{x}_{n+1})|, \tag{24}$$

where  $\hat{m}_i(\mathbf{x}_{n+1}) = \mathbb{E}[f(\mathbf{x}_{n+1}, \hat{V}_i)]$ , we denote by  $|\cdot|$  the absolute value function. In the following, the *stopping criterion* is defined by the following relation,

$$\forall 0 \leq j \leq l_0, e_{l-j}(\mathbf{x}_{n+1}) \leq \varepsilon \tag{25}$$

It ensures that the quantities  $e_l$  are smaller than a prescribed tolerance  $\varepsilon$  on the  $l_0$  previous steps in the estimation. These two parameters are set by practitioners. It allows using fewer curves without losing estimation accuracy.

**Remark** The parameters  $(l_0, \varepsilon)$  are closely linked to the allocated budget. Moreover, the parameter  $l_0$  can be set in practice between 2 and 5 regarding the stability we want to achieve with the method. About the parameter  $\varepsilon$ , it will be

intuitively calibrated depending both on the precision and on the scale of the outputs.

The strategy SUR could be stopped if the allocated number of simulations is reached. However, we define in this work an additional stopping criterion based on the Vorob'ev deviation and close to the one defined for the expectation estimate. Thus, the strategy is carried out until the following stopping criterion is verified

$$\forall 0 \leq j \leq l_0^{\text{SUR}}, e_{l-j}^{\text{SUR}}(\mathbf{x}_{n+1}) \leq \varepsilon^{\text{SUR}}, \tag{26}$$

where  $e_i^{\text{SUR}} = |\mathbb{E}_{i-1}[\mu(\Gamma \Delta Q_{i-1, \alpha_{i-1}^*})] - \mathbb{E}_i[\mu(\Gamma \Delta Q_{i, \alpha_i^*})]|$  is the absolute error between two successive Vorob'ev deviations. The condition Eq. (26) tests whether all the quantities are smaller than a tolerance  $\varepsilon^{\text{SUR}}$  on  $l_0^{\text{SUR}}$  consecutive steps. Alternatively, one might consider a stopping criterion based on the values rather than the variations of the Vorob'ev deviation. This criterion is given by

$$\forall 0 \leq j \leq l_0^{\text{SUR}}, \mathbb{E}_{l-j}[\mu(\Gamma \Delta Q_{i-1, \alpha_{i-j}^*})] \leq \varepsilon^{\text{SUR}}.$$

The global methodology to perform inversion in the presence of functional uncertainty proposed in this paper is summarized in Algorithm 4.

**Algorithm 4** Data-driven stochastic inversion under functional uncertainties

- 1: Create an initial design of experiments (DoE) of  $n$  points in the control space  $\mathbb{X}$ .
- 2: Alg  $\mathcal{A} \leftarrow$  choose one of the Algorithms 1,2 and 3.
- 3: Estimate the expectation (Alg.  $\mathcal{A}$ ).
- 4: Deduce  $\{\tau_i^2\}_{i=1}^n$  (if Crude MC or FPCA methods).
- 5: **while** Stopping criterion Eq. (26) not met (SUR) **do**
- 6:    $\mathbf{x}_{n+1} \leftarrow$  Sampling criterion  $\mathcal{I}_n$ .
- 7:   Set  $l = 1$ .
- 8:   **while** Stopping criterion Eq. (25) not met (Expectation Estimation) **do**
- 9:     Approximate the expectation by  $\mathbb{E}[f(\mathbf{x}_{n+1}, \hat{V}_l)]$  (Alg.  $\mathcal{A}$ ).
- 10:     Set  $l = l + 1$ .
- 11:   **end while**
- 12:    $\tau_{\mathbf{x}_{n+1}}^2 \leftarrow \text{var}(f(\mathbf{x}_{n+1}, \hat{V}_l))$  (if Crude MC or FPCA methods).
- 13:   Update DoE.
- 14:   Set  $n = n + 1$ .
- 15: **end while**
- 16: **end**

*Remark on stage 2 of Algorithm 4* Due to their sampling-based nature, the Crude MC and FPCA methods are sensitive to the resulting estimation errors. Consequently, we consider the adaptation of the SUR strategy for noisy observations (see Sect. 4.3).

## 6 Numerical tests

In this section, we apply the proposed data-driven methodology for stochastic inversion under functional uncertainties to two test cases. On an analytical test case, we first highlight through a comparison to a random infill strategy the effectiveness of the SUR strategy. Secondly, we compare the methods combining the SUR strategy to the four approaches to estimate the expectation. We then present in Sect. 6.2 an application to the industrial automotive test case which motivates our study.

### 6.1 Analytical example

To compare the SUR strategy to a random infill one, we define a deterministic function  $f_{determ}$  as follows:

$$f_{determ} : \mathbf{x} \mapsto \max_t \mathbf{v}_{determ} \cdot |0.1 \cos(x_1 \max_t \mathbf{v}_{determ}) \cdot \sin(x_2) \cdot (x_1 + x_2 \min_t \mathbf{v}_{determ})^2| \cdot \int_0^T (30 + \mathbf{v}_{determ})^{\frac{x_1 - x_2}{20}} dt,$$

where the control variable  $\mathbf{x}$  lies in  $\mathbb{X} = [1.5, 5] \times [3.5, 5]$  and  $\mathbf{v}_{determ}$  is a fixed curve. We are interested in the set  $\Gamma^* := \{\mathbf{x} \in \mathbb{X}, f_{determ}(\mathbf{x}) \leq 0.2\}$ . We consider a Gaussian process prior with constant mean function and Matérn covariance kernel with  $\nu = 5/2$ . A Random Latin Hypercube design was used as an initial DoE for both strategies creating new initial design with nine points for every run. In Fig. 8, one can see the evolution of the Vorob'ev deviation and the set estimation error when new points are added. We observe that the SUR strategy manages to quickly reduce the Vorob'ev deviation (top plot) and that the Vorob'ev expectation obtained after the new evaluations matches with the true set. This example illustrates that a random filling strategy may not be optimal for set estimation, as it clearly was outperformed by the adaptive SUR strategy.

We now consider the function  $f(\mathbf{x}, \mathbf{V})$  with  $\mathbf{V}$  is a standard Brownian motion. We suppose that a sample of  $N$  realizations of  $\mathbf{V}$  is available, denoted by  $\mathcal{E}$ , and these realizations are discretized uniformly on 100 points. The objective is to construct the set  $\Gamma^* := \{\mathbf{x} \in \mathbb{X}, g(\mathbf{x}) = \mathbb{E}_{\mathbf{V}}[f(\mathbf{x}, \mathbf{V})] \leq c\}$ , where  $c = 1.2$ .

Here, we consider a Gaussian process prior  $(Y_{\mathbf{x}})_{\mathbf{x} \in \mathbb{X}} \sim GP(m, k)$ , with constant mean function and Matérn covariance kernel with  $\nu = 5/2$ . The initial DoE consists of a nine-points Latin Hypercube Sample (LHS) design optimized by maximin criterion. The hyper-parameters of the Gaussian process  $Y$  are estimated by Maximum Likelihood Estimation (MLE). Figure 9 shows the initial design of experiments and the target set  $\Gamma^*$  obtained from a  $30 \times 30$  grid experiment, where at each grid point the expectation is approximated by a Monte Carlo Method over 5000 realiza-

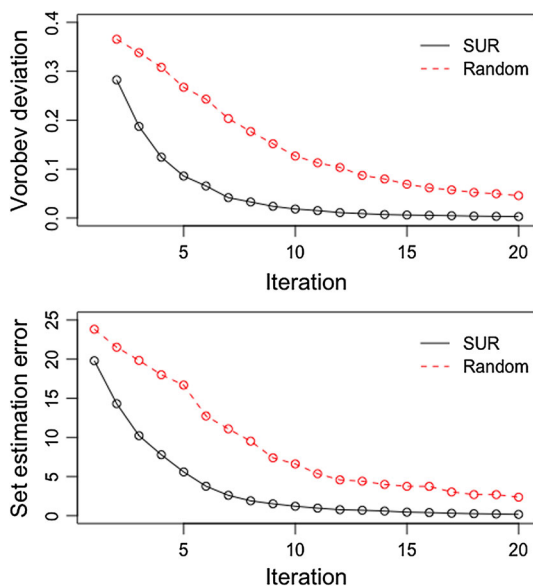


**Fig. 8** Analytical example. The average Vorob'ev deviation (top) and the average set estimation error  $\mu(\Gamma^* \Delta Q_{iter, \alpha_{iter}^*}) / \mu(\Gamma^*)$  (bottom) using 30 independent runs

tions of  $V$ . We aim at estimating the set  $\Gamma^*$  using the SUR strategy to choose the next evaluation point as defined in Sect. 4, and the methods presented in Sect. 2 to provide an efficient estimation of the expectation. We proceed to add one point at each iteration of the SUR strategy until the condition Eq. (26) for  $(l_0^{SUR}, \varepsilon^{SUR}) = (4, 5 \times 10^{-3})$  is reached. The covariance parameters are re-estimated at each step by MLE. Since this criterion is based on the Vorob'ev deviation, the objective is to reduce the uncertainty on the set estimate until stability. For the sequential estimation of the expectation, we test the sensitivity to the parameters  $(l_0, \varepsilon)$  of criterion Eq. (25) (see Table 1).

The estimation of the expectation at the proposed point by SUR is carried out with one of the methods detailed in Sect. 2 (FPCA, crude MC, maximin-GFQ,  $\mathbb{L}^2$ -GFQ). As presented in Sect. 5, the estimation is done sequentially and it depends on the *stopping criteria* parameters  $l_0, \varepsilon$  and on the truncation argument  $m_{KL}$ . This latter is set at  $m_{KL} = 7$  in order to explain 97% of the variance. The four expectation estimation methods are sequential as detailed in Sect. 2. Indeed, the two GFQ methods are sequential by definition. The crude MC method is sequential because at each step, a curve is drawn with replacement from the available sample  $\mathcal{E}$  (see Algorithm 3). The same goes for the probabilistic approach (FPCA); at each step, we add a new curve built as already explained.

The first test consists in fixing the available sample of realizations of  $V$  ( $N = 200$ ). For this fixed sample, we compare the obtained results for different  $l_0$  and  $\varepsilon$ . Table 1 lists the parameters tested in this section.

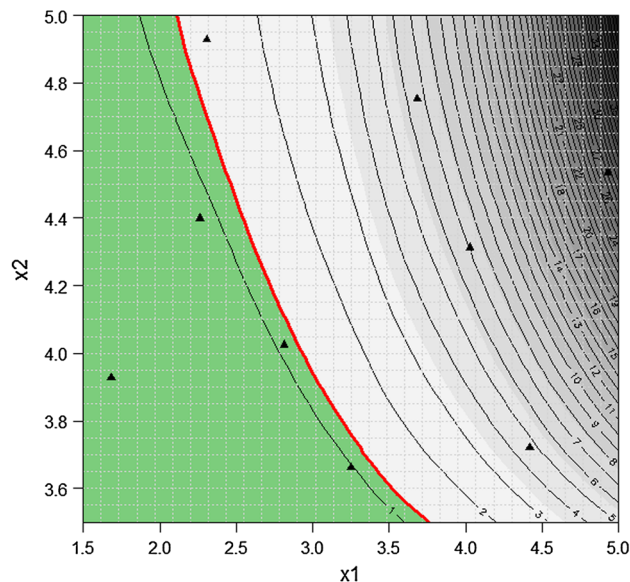


**Fig. 9** Analytical example. Contour plot of the function  $g$ , the set of interest (green) with boundary (red line), the initial design of experiments (black triangles). (Colour figure online)

**Table 1** Analytical example. Estimation of expectation *stopping criteria* parameters

$l_0$	4	2	3	4
$\varepsilon$	$10^{-2}$	$5 \times 10^{-3}$	$5 \times 10^{-3}$	$5 \times 10^{-3}$

To compare the performance of the various methods, we use the ratio between the volume of the symmetric difference between the true set  $\Gamma^*$  and the estimated set at last iteration,  $\mu(\Gamma^* \Delta Q_{n_{last}, \alpha_{n_{last}}^*})$  and the volume of the true set,  $\mu(\Gamma^*)$ . As shown earlier in Fig. 6, the maximin-GFQ method is not very sensitive to the starting point. Thus, in the following test, we consider the deterministic version of the maximin-GFQ method by fixing the starting point to the one of  $\mathbb{L}^2$ -GFQ method.

From the comparison results displayed in Table 2 and plotted on Fig. 10, we note that the two GFQ methods are sensitive to the parameters  $l_0$  and  $\varepsilon$ . The  $\mathbb{L}^2$ -GFQ method performs well in set estimation error terms, and the maximin-GFQ provides better results in terms of cost. In the following comparison tests, we consider only the  $\mathbb{L}^2$ -GFQ method as it gives much better set estimation error for a reasonable number of calls to the function  $f$ .

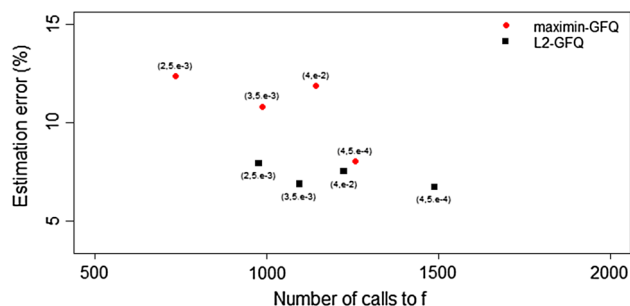
Regarding the second test, the two expectation estimation methods (Crude MC and FPCA) have a stochastic behaviour because of the sampling steps. To account for these variabilities, the performance of each method is averaged over 30 independent runs. The results are summarized in Tables 3 and 4. The results indicate that the three methods are sensitive to the parameters  $l_0$  and  $\varepsilon$ : larger is the parameter  $l_0$ ,

**Table 2** Analytical example. (Top) The relative error obtained by the two GFQ methods for different values of  $l_0$  and  $\varepsilon$ . (Bottom) The cumulative number of calls to the function  $f$  (in brackets are the number of iterations required to reach the stopping criterion in the SUR strategy)

$(l_0, \varepsilon)$	$\mu(\Gamma^* \Delta Q_{n_{1ast}, \alpha_{n_{1ast}}^*}) / \mu(\Gamma^*)$	
	Maximin-GFQ (%)	$\mathbb{L}^2$ -GFQ (%)
(4, 1.e-2)	11.86	7.50
(2, 5.e-3)	12.34	7.93
(3, 5.e-3)	10.80	6.87
(4, 5.e-3)	8.02	6.79

$(l_0, \varepsilon)$	Cumulative number of calls to $f$	
	Maximin-GFQ	$\mathbb{L}^2$ -GFQ
(4,1.e-2)	1144 (21)	1225 (42)
(2,5.e-3)	735 (21)	978 (22)
(3,5.e-3)	989 (18)	1096 (21)
(4,5.e-3)	1259 (19)	1489 (26)



**Fig. 10** Analytical example. The relative error obtained by the two GFQ methods for different values of  $l_0$  and  $\varepsilon$  as a function of the number of calls to the function  $f$

**Table 3** Analytical example. The average relative error obtained by the crude MC, FPCA for different values of  $l_0$  and  $\varepsilon$  (in brackets are the standard deviation for the crude MC and FPCA methods)

$(l_0, \varepsilon)$	$\mu(\Gamma^* \Delta Q_{n_{1ast}, \alpha_{n_{1ast}}^*}) / \mu(\Gamma^*)$		
	Crude MC	FPCA	$\mathbb{L}^2$ -GFQ (%)
(4, 1.e-2)	9.53% (4.12)	9.89% (4.14)	<b>7.50</b>
(2, 5.e-3)	9.84% (3.24)	10.86% (2.82)	<b>7.93</b>
(3, 5.e-3)	9.54% (3.81)	7.29% (1.07)	<b>6.87</b>
(4, 5.e-3)	8.98% (2.62)	7.01% (1.21)	<b>6.79</b>

Best values are shown in bold

i.e. when seeking to a stability of the estimation, smaller is the error but higher is the number of calls to the function  $f$ . The  $\mathbb{L}^2$ -GFQ method performs well in terms of error and cost. The cumulative number of calls to  $f$  has been decreased by a factor greater than 3 in comparison with the two other methods.

**Table 4** Analytical example. The average cumulative number of calls to the function  $f$  (written in brackets are the number of iterations required to reach the stopping criterion in the SUR strategy)

$(l_0, \varepsilon)$	Cumulative number of calls to the function $f$		
	Crude MC	FPCA	$\mathbb{L}^2$ -GFQ
(4, 1.e-2)	2849 (27)	2805 (24)	<b>1225 (42)</b>
(2, 5.e-3)	2393 (26)	2670 (23)	<b>978 (22)</b>
(3, 5.e-3)	3537 (23)	3661 (20)	<b>1096 (21)</b>
(4, 5.e-3)	4400 (23)	4278 (20)	<b>1489 (26)</b>

Best values are shown in bold

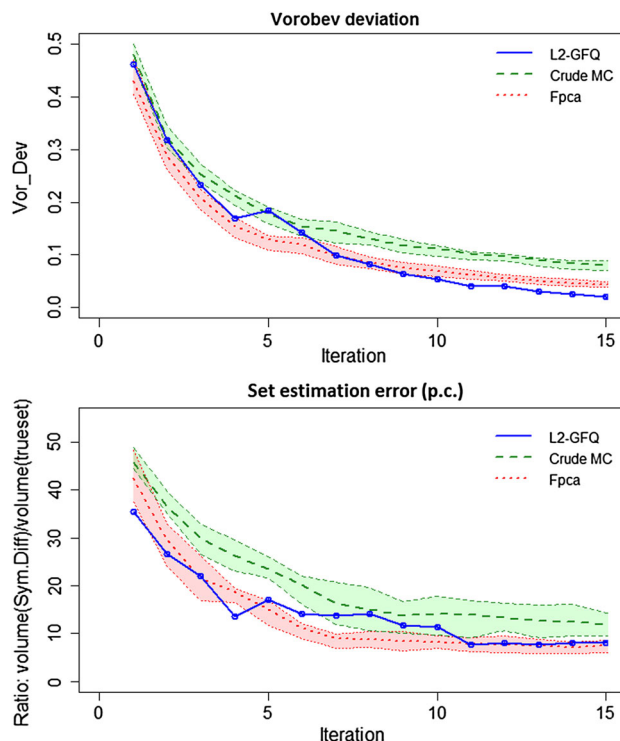


**Fig. 11** Analytical example. Results for  $(l_0, \varepsilon) = (4, 5.e^{-3})$ . Lines denote the average, and coloured bands mark the 25-th and 75-th quantiles [FPCA (in red) and Crude MC (in green)]. Top: The Vorob'ev deviation. Bottom: the set estimation error  $\mu(\Gamma^* \Delta Q_{n_{1ast}, \alpha_{n_{1ast}}^*}) / \mu(\Gamma^*)$

Figure 11 shows the set estimation error and the Vorob'ev deviation as a function of the iteration number for the three methods and  $(l_0, \varepsilon) = (4, 5.e^{-3})$ . For the crude MC and FPCA methods, the dotted lines indicate average error decay, and the coloured bands mark the area between the 25th and 75th error quantiles. Note that the three methods show a strong decrease in the set estimation error. The main observation that can be made is that, for a small total number of calls to  $f$  (see, Table 4), the convergence rate for the proposed approach ( $\mathbb{L}^2$ -GFQ) is better in comparison with the Crude MC and FPCA methods.

In the following, the stopping criteria for SUR ( $l_0^{SUR} = 4, \varepsilon^{SUR} = 5 \times 10^{-3}$ ) and for the expectation estimation

**Table 5** Analytical example. (Top) The average set estimation error obtained for different sample sizes and methods and  $m_{KL} = 7$  (in brackets are the standard deviation). (Bottom) The average cumulative number of calls to the function  $f$  (in brackets are the number of iterations required to reach the stopping criterion in the SUR strategy)

	$\mu(\Gamma^* \Delta Q_{n_{last}, \alpha_{n_{last}}^*}) / \mu(\Gamma^*)$		
	Crude MC	FPCA	$\mathbb{L}^2$ -GFQ
$N = 50$	15.38% (8.76)	13.25% (5.09)	<b>11.13%</b> (6.48)
$N = 100$	9.60% (4.65)	9.08% (5.41)	<b>8.80%</b> (3.60)
$N = 200$	8.22% (2.18)	7.71% (2.35)	<b>7.02%</b> (2.31)
	Cumulative number of calls to $f$		
	Crude MC	FPCA	$\mathbb{L}^2$ -GFQ
$N = 50$	4281 (22)	4343 (21)	<b>1044</b> (27)
$N = 100$	4262 (22)	4313 (21)	<b>1236</b> (25)
$N = 200$	4152 (22)	4552 (21)	<b>1262</b> (24)

Best values are shown in bold

( $l_0 = 4, \varepsilon = 5 \times 10^{-3}$ ) are chosen in order to offer a good compromise between the accuracy and the number of model evaluations.

Table 5 compares the sensitivity of the methods to the size of the available sample  $\mathcal{E}$ , denoted by  $N$ . In each cell of the table, we perform  $20 \times 20$  independent runs. Indeed, for each value of  $N$ , we generate 20 training samples  $\mathcal{E}$  of size  $N$ , and for each sample, we perform 20 runs for each method. The table summarizes the results averaged over the 400 runs.

We note that for a larger sample size, the recovering error is smaller. This can be explained by the fact that with a large sample size, the available information on variable  $V$  enables an effective estimation of the expectation.

We know that the  $\mathbb{L}^2$ -GFQ and the probabilistic modelling (FPCA) depend on the truncation argument. To better understand the effect of the number of dimensions  $m_{KL}$ , we fix the stopping criteria for the SUR strategy and expectation estimation, and we consider different values of  $m_{KL} = \{2, 3, 4, 5, 6\}$ . Each cell of Table 6 represents the result averaged over  $14 \times 20$  independent runs. For each  $m_{KL}$ , we generate 14 samples  $\mathcal{E}$  of size  $N=200$ , and for each of them, we perform 20 runs of each method.

Table 6 shows that for all values of  $m_{KL}$ , the  $\mathbb{L}^2$ -GFQ method outperforms the probabilistic FPCA modelling. As shown in Table 7, for high truncation argument, the explained variance increases, which explains the decrease in the estimation error for the probabilistic modelling (FPCA). On the other hand, the  $\mathbb{L}^2$ -GFQ accuracy seems to be almost constant for  $m_{KL} \geq 3$ . This can be explained by the fact that the KL expansion is only used to define a space-filling design, and the information lost by the truncation is recovered by taking the corresponding curve in the set  $\mathcal{E}$ . On the contrary, the probabilistic modelling which is based on FPCA gives better

**Table 6** Analytical example. (Top) The average set estimation error obtained by the FPCA and the  $\mathbb{L}^2$ -GFQ methods for different values of  $m_{KL}$  (in brackets are the standard deviation). (Bottom) The average cumulative number of calls to the function  $f$  (in brackets are the number of iterations required to reach the stopping criterion in the SUR strategy)

	$\mu(\Gamma^* \Delta Q_{n_{last}, \alpha_{n_{last}}^*}) / \mu(\Gamma^*)$	
	FPCA	$\mathbb{L}^2$ -GFQ
$m_{KL} = 2$	11.43% (3.70)	<b>8.90%</b> (3.71)
$m_{KL} = 3$	10.70% (3.38)	<b>7.72%</b> (3.38)
$m_{KL} = 4$	9.24% (3.18)	<b>7.40%</b> (3.13)
$m_{KL} = 5$	8.94% (2.66)	<b>7.05%</b> (5.09)
$m_{KL} = 6$	8.27% (1.67)	<b>6.96%</b> (3.32)
	Cumulative number of calls to $f$	
	FPCA	$\mathbb{L}^2$ -GFQ
$m_{KL} = 2$	3855 (18)	<b>1286</b> (26)
$m_{KL} = 3$	4418 (24)	<b>1139</b> (21)
$m_{KL} = 4$	4438 (21)	<b>1236</b> (20)
$m_{KL} = 5$	4542 (21)	<b>1214</b> (25)
$m_{KL} = 6$	4955 (19)	<b>1142</b> (21)

Best values are shown in bold

**Table 7** Analytical example. The explained variance in the function of  $m_{KL}$

$m_{KL}$	2	3	4	5	6
Explained variance	90.2%	93.4%	95.1%	96%	96.7%

results for higher  $m_{KL}$ . However, the errors in Table 6 seem to be bounded below. To go below that bound, we probably need to increase the size of  $\mathcal{E}$ . Figure 12 shows the estimation of the true set based on the initial design of experiments, and Fig. 13 shows the results at the last iteration.

### 6.2 IFPEN test case

In this section, we test the proposed method on an automotive test case from IFPEN (IFP Energies Nouvelles). The problem concerns an after-treatment device of diesel vehicles, called Selective Catalytic Reduction (SCR). This latter consists on a basic process of chemical reduction of nitrogen oxides ( $\text{NO}_x$ ) to diatomic nitrogen ( $\text{N}_2$ ) and water ( $\text{H}_2\text{O}$ ) by the reaction of  $\text{NO}_x$  and ammonia  $\text{NH}_3$ . The reaction itself occurs in the SCR catalyst. Ammonia is provided by a liquid-reductant agent injected upstream of the SCR catalyst. The amount of ammonia introduced into the reactor is a critical quantity: overdosing causes undesirable ammonia slip downstream of the catalyst, whereas underdosing causes insufficient  $\text{NO}_x$  reduction. In practice, ammonia slip is restricted to a prescribed threshold.

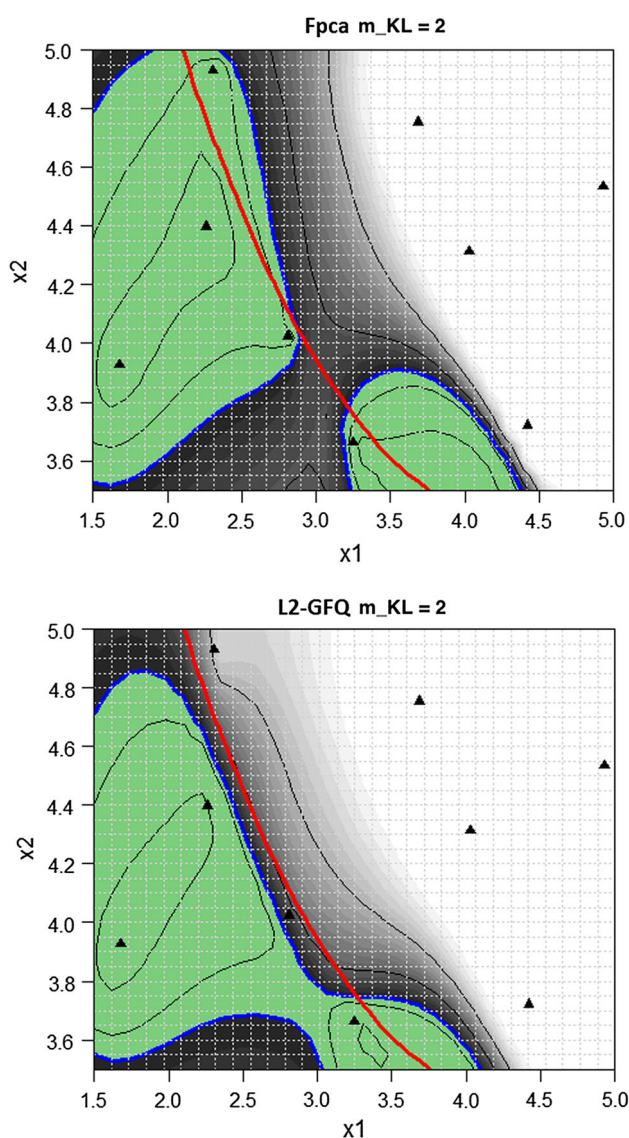


**Fig. 12** Analytical example. Results based on the initial DoE in the case  $m_{KL} = 2$ . The coverage function, the boundary of the true set (red), the estimated sets (green)

We use an emission-oriented simulator developed by IFPEN, which models the vehicle, its engine and the exhaust after-treatment system. It takes the vehicle-driving cycle profile as input and provides the time series of corresponding exhaust emissions as output. A realistic SCR control law is used in this simulator. See Bonfils et al. (2012) for an example of such a control law. In this study, we choose two control variables as input and a functional one considered as random. The control variables are parameters of the SCR control law. They set the targeted level of  $\text{NH}_3$  storage in the catalyst and then are indirectly related to the  $\text{NH}_3$  injected. They lie in  $\mathbb{X} = [0, 0.6]^2$ . The functional random variable describes the evolution of vehicle speed on  $I$ , with  $I = [0, 5400 \text{ s}]$ . These functional uncertainties come from an available sample of 100 real-driving cycles. Regarding the discretization of the

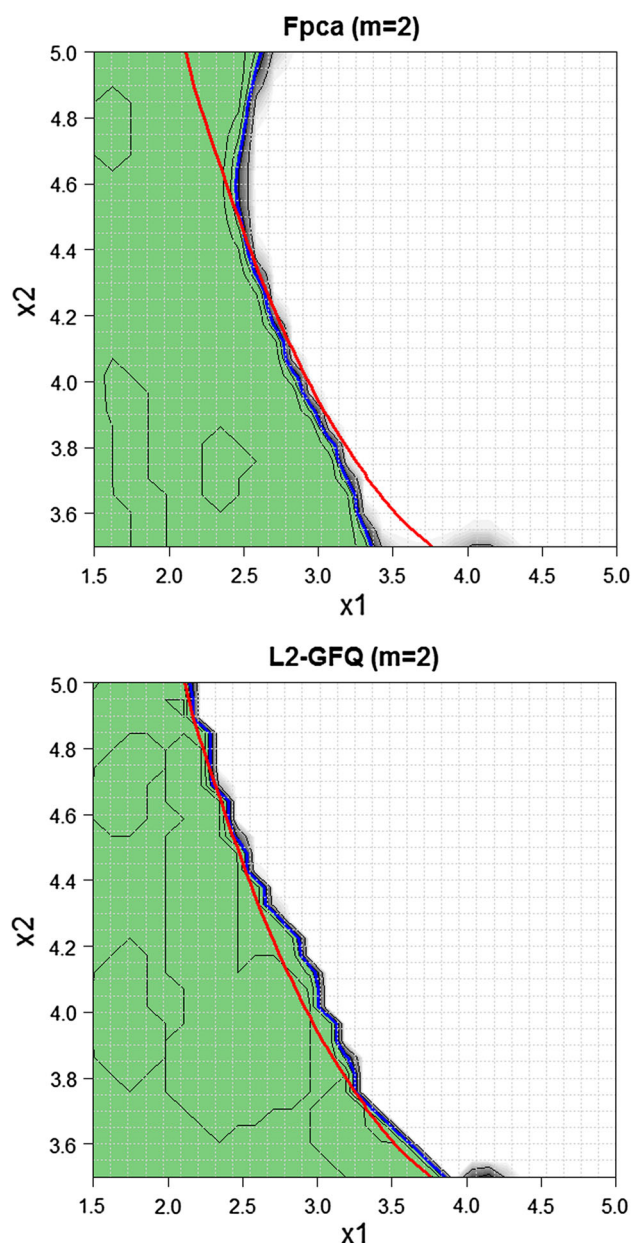


**Fig. 13** Analytical example. Results at the last iteration in the case  $m_{KL} = 2$ . The coverage function, the boundary of the true set (red), the estimated sets (green)

real-driving cycle, we have one observation per second, so  $\forall i \in \{1, \dots, 100\}$ ,  $\mathbf{v}_i \in \mathbb{R}^{5400}$ . A subset of that sample is represented in Fig. 14. In this setting, the functional PCA takes about 3 min.

In short, the ammonia emissions peak during a driving cycle is modelled as a function,

$$f : \mathbb{X} \times \mathcal{V} \rightarrow \mathbb{R} \\ (x, \mathbf{V}) \mapsto f(x, \mathbf{V}) = \max_{t \in I} \text{NH}_3^{\text{slip}}(t)$$

We are interested in recovering the set  $\Gamma^* = \{x \in \mathbb{X}, g(x) = \mathbb{E}_{\mathbf{V}}[f(x, \mathbf{V})] \leq c\}$ , with  $c = 30 \text{ ppm}$ . Conducting this study

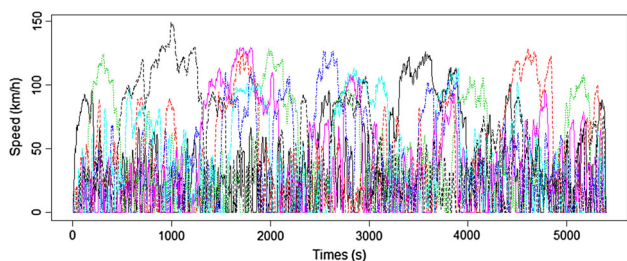


Fig. 14 Automotive test case. Sample of seven real-driving cycles

on a full grid would consist in covering the space  $[0, 0.6]^2$  with a fine mesh and evaluating the code 100 times at each point. Knowing that each simulation takes about 2 min, such study would require many computational hours, and thus, the use of meta-models allows to tackle this computational issue.

Here, we consider a Gaussian process prior  $(Y_x)_{x \in \mathbb{X}} \sim GP(m, k)$ , with constant mean function and Matérn covariance kernel with  $\nu = 5/2$ . The initial DoE consists of a eight-points LHS design optimized with respect to the maximin criterion. The covariance kernel hyper-parameters are estimated by maximizing the likelihood.

As for the analytical example, we proceed to add one point at each iteration for the SUR strategy until the stopping criterion with  $(l_0^{SUR}, \epsilon^{SUR}) = (4, 5 \times 10^{-3})$  is verified. Concerning the expectation estimation, we set the stopping criterion parameters at  $(l_0, \epsilon) = (4, 10^{-2})$  and the truncation argument is set at  $m_{KL} = 20$  in order to explain 80% of the variance. The algorithm was stopped at the 62-point design because the Vorob’ev deviation appears as stabilized, in other words, the absolute error between the Vorob’ev deviations of the points 58–62 is smaller than 0.005, as shown in Fig. 15. We note that for each additional point, the new observed response affects the estimation of the excursion set and its uncertainty. Thus, although the Vorob’ev deviation generally decreases, it is not a monotonic decreasing. The stopping criterion is constructed to check the stability of convergence by taking into account the last four iterations.

In searching for the true set, the SUR algorithm heavily visits the boundary region of  $\Gamma^*$  and explores also potentially interesting regions (cf. Fig. 16). In each added point, Fig. 16 shows the number of necessary driving cycles to estimate the expectation. We remark that instead of taking the whole sample (100 driving cycles), it was sufficient to sequentially and wisely choose a reduced and representative number of driving cycles below 35. In the present case, the excursion domain  $\Gamma^*$  is well recovered by the algorithm. Actually, after 62 iterations (1575 evaluations) the whole domain  $\mathbb{X}$  has an excursion probability close to either 0 or 1.

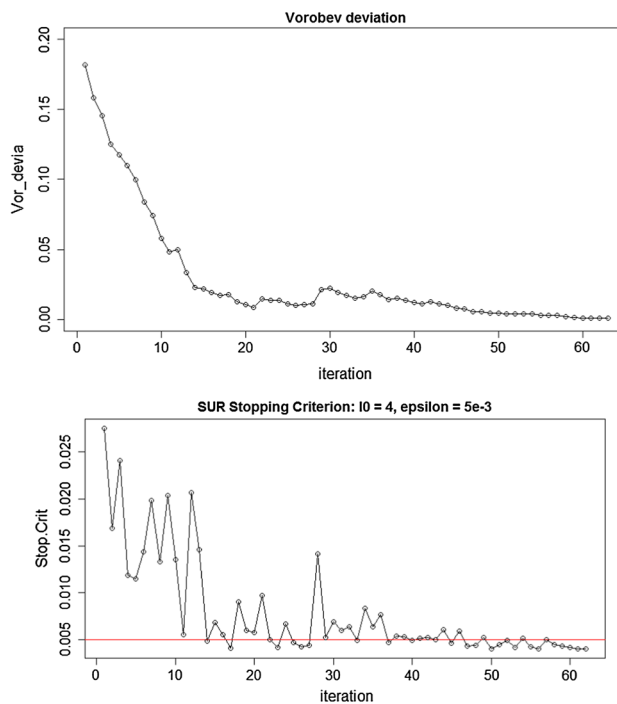


Fig. 15 Automotive test case. Top: decrease in the Vorob’ev deviation at each iteration when new points are added. Bottom: evolution of the absolute error Eq. (26) and the red line represents the stopping criterion

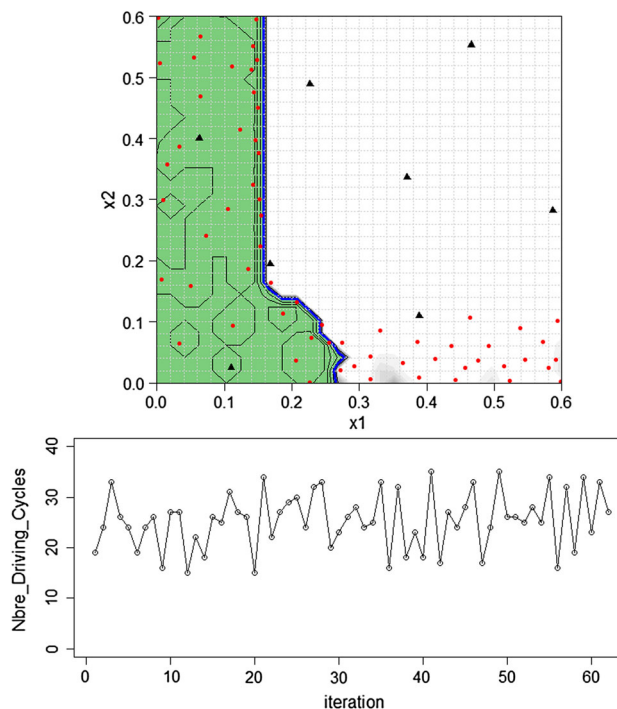


Fig. 16 Automotive test case. Left: coverage probability function (grey scale), estimate set (green) after 62 added points and 1575 function evaluations, initial DoE (black triangles), the sequentially added points (red circles). Right: number of driving cycles used to estimate expectation at each added point

## 7 Conclusions

In this paper, a new method of inversion under uncertainty was proposed for problems where some of the input parameters are functional random variables with unknown probability distribution. (Only a sample is available.) The objective is to recover the set of control variables leading to robustly ensure some constraints by taking into account the uncertainties. The method is composed of two steps : a sequential strategy to estimate the excursion set and the modelling of functional uncertainties. To solve the first issue, a kriging model in the control input space is built. It makes possible to assess the uncertainty on the set of interest given a sample of evaluations. Then, a sequential strategy (SUR) proposed by Chevalier et al. (2013) and based on the kriging model is used to sequentially and efficiently choose new evaluation points to improve the excursion set estimation. For the second issue, we consider the expectation to model uncertainties and we propose two sequential approaches to estimate the expectation at each point proposed by SUR. Each curve is represented by its coefficients in a truncated KL decomposition. The chosen points in the KL coefficients finite set, each one corresponding to a curve, are sequentially added and chosen either to approximate a maximin space-filling design or to reduce the quantization error. This methodology leads to an efficient estimation of the expectation, as illustrated on the application on an analytical test case with two control inputs and a functional random one. The results illustrate significant enhancement in terms of precision and number of calls to the simulator. We also applied this method to the automotive test case which motivated this research work. The obtained result agrees with the intuitions made from physics behind the simulator. The paper focuses on the mean of  $f(x, \mathbf{V})$ , and here we choose to construct a GP model for the unobservable integrated response  $g$ . In the optimization context and for discrete and continuous random variables, existing works deal with the case of unobservable response (see Williams et al. 2000; Janusevskis and Le Riche 2013). The authors propose to build a GP model for the simulator  $f$  and induce a new GP model by integrating the previous one over the distribution of the uncertain variables. The adaptation of these works in the context of inversion and functional random variables is an on-going work. Other functionals of the output distribution may also be of great importance. For example, practitioners may be interested in ensuring a certain level of reliability, leading to consider a probabilistic constraint. The proposed method could be adapted to that case by seeing the probability as an expectation, at least for moderate risk levels.

**Acknowledgements** The authors would like to thank the anonymous reviewers and the associate editor for their helpful comments which substantially improved this paper. We also thank the Inria Associate

Team UNcertainty QUantification is ESenTial for Oceanic & Atmospheric flows proBLEms. This work was supported by IFPEN and the OQUAIDO chair.

## References

- Abtini, M.: Plans prédictifs à taille fixe et séquentiels pour le krigage. Ph.D. thesis, Ecole Centrale Lyon (2018)
- Bect, J., Ginsbourger, D., Li, L., Picheny, V., Vazquez, E.: Sequential design of computer experiments for the estimation of a probability of failure. *Stat. Comput.* **22**(3), 773–793 (2012)
- Bect, J., Bachoc, F., Ginsbourger, D.: A supermartingale approach to Gaussian process based sequential design of experiments. *arXiv preprint arXiv:1608.01118* (2016)
- Bolin, D., Lindgren, F.: Excursion and contour uncertainty regions for latent Gaussian models. *J. R. Stat. Soc. Ser. B (Stat. Methodol.)* **77**(1), 85–106 (2015)
- Bonfils, A., Creff, Y., Lepreux, O., Petit, N.: Closed-loop control of a SCR system using a NO<sub>x</sub> sensor cross-sensitive to NH<sub>3</sub>. *IFAC Proc. Vol.* **45**(15), 738–743 (2012)
- Cardot, H., Ferraty, F., Sarda, P.: Functional Linear Model. *Stat. Probab. Lett.* **45**(1), 11–22 (1999)
- Chevalier, C.: Fast uncertainty reduction strategies relying on Gaussian process models. Ph.D. thesis (2013)
- Chevalier, C., Ginsbourger, D.: Fast Computation of the multi-points expected improvement with applications in batch selection. In: *International Conference on Learning and Intelligent Optimization*, pp. 59–69. Springer (2013)
- Chevalier, C., Ginsbourger, D., Bect, J., Molchanov, I.: Estimating and quantifying uncertainties on level sets using the Vorob'ev expectation and deviation with Gaussian process models. In: *mODA 10—Advances in Model-Oriented Design and Analysis*, pp. 35–43. Springer (2013)
- Chevalier, C., Picheny, V., Ginsbourger, D.: Kriginv: an efficient and user-friendly implementation of batch-sequential inversion strategies based on kriging. *Comput. Stat. Data Anal.* **71**, 1021–1034 (2014a)
- Chevalier, C., Bect, J., Ginsbourger, D., Vazquez, E., Picheny, V., Richet, Y.: Fast parallel kriging-based stepwise uncertainty reduction with application to the identification of an excursion set. *Technometrics* **56**(4), 455–465 (2014b)
- Chevalier, C., Emery, X., Ginsbourger, D.: Fast update of conditional simulation ensembles. *Math. Geosci.* **47**(7), 771–789 (2015)
- Flury, B.A.: Principal points. *Biometrika* **77**(1), 33–41 (1990)
- French, J.P., Sain, S.R., et al.: Spatio-temporal exceedance locations and confidence regions. *Ann. Appl. Stat.* **7**(3), 1421–1449 (2013)
- Jackson, D.A.: Stopping rules in principal components analysis: a comparison of heuristical and statistical approaches. *Ecology* **74**(8), 2204–2214 (1993)
- Janusevskis, J., Le Riche, R.: Simultaneous kriging-based estimation and optimization of mean response. *J. Glob. Optim.* **55**(2), 313–336 (2013)
- Jin, R., Chen, W., Sudjianto, A.: An efficient algorithm for constructing optimal design of computer experiments. *J. Stat. Plan. Inference* **134**(1), 268–287 (2005)
- Johnson, M.E., Moore, L.M., Ylvisaker, D.: Minimax and maximin distance designs. *J. Stat. Plan. Inference* **26**(2), 131–148 (1990)
- L'Ecuyer, P., Lemieux, C.: Recent advances in randomized quasi-Monte Carlo methods. In: Dror, M., L'Ecuyer, P., Szidarovszky, F. (eds.) *Modeling Uncertainty*, pp. 419–474. Springer, Berlin (2005)
- L'Ecuyer, P., Owen, A.B.: *Monte Carlo and Quasi-Monte Carlo Methods 2008*. Springer, Berlin (2009)
- Levrard, C.: High-dimensional vector quantization: convergence rates and variable selection. Ph.D. thesis, Université de Paris 11 (2014)

- Luschgy, H., Pagès, G.: Greedy vector quantization. *J. Approx. Theory* **198**, 111–131 (2015)
- Luschgy, H., Pagès, G., Wilbertz, B.: Asymptotically optimal quantization schemes for Gaussian processes on Hilbert spaces. *ESAIM Probab. Stat.* **14**, 93–116 (2010)
- Miranda, M., Bocchini, P.: Functional Quantization of stationary Gaussian and non-Gaussian random processes. In: Deodatis, G., Ellingwood, B.R., Frangopol, D.M. (eds.) *Safety, Reliability, Risk and Life-Cycle Performance of Structures and Infrastructures*, pp. 2785–2792. CRC Press/Balkema, London (2013)
- Miranda, M.J., Bocchini, P.: A versatile technique for the optimal approximation of random processes by functional quantization. *Appl. Math. Comput.* **271**, 935–958 (2015)
- Morris, M.D., Mitchell, T.J.: Exploratory designs for computational experiments. *J. Stat. Plan. Inference* **43**(3), 381–402 (1995)
- Nanty, S., Helbert, C., Marrel, A., Pérot, N., Prieur, C.: Sampling, meta-modeling, and sensitivity analysis of numerical simulators with functional stochastic inputs. *SIAM/ASA J. Uncertain. Quantif.* **4**(1), 636–659 (2016)
- Pagès, G.: Introduction to optimal vector quantization and its applications for numerics. Tech. rep. (2014). <https://hal.archives-ouvertes.fr/hal-01034196>
- Pagès, G., Printems, J.: Functional quantization for numerics with an application to option pricing. *Monte Carlo Methods Appl. mcma* **11**(4), 407–446 (2005)
- Pagès, G., Printems, J.: Optimal quantization for finance: from random vectors to stochastic processes. In: Bensoussan, A., Zhang, Q. (eds.) *Handbook of Numerical Analysis*, vol. 15, pp. 595–648. Elsevier, Amsterdam (2009)
- Picheny, V., Ginsbourger, D., Roustant, O., Haftka, R.T., Kim, N.H.: Adaptive designs of experiments for accurate approximation of a target region. *J. Mech. Des.* **132**(7), 071008 (2010)
- Pronzato, L., Müller, W.G.: Design of computer experiments: space filling and beyond. *Stat. Comput.* **22**(3), 681–701 (2012)
- Ramsay, J.O.: *Functional Data Analysis*. Wiley Online Library, New York (2006)
- Roustant, O., Ginsbourger, D., Deville, Y.: DiceKriging, DiceOptim: Two R packages for the analysis of computer experiments by Kriging-based metamodeling and optimization. *J. Stat. Softw.* **51** (2013)
- Vazquez, E., Bect, J.: A sequential Bayesian algorithm to estimate a probability of failure. *IFAC Proc.* Vol. **42**(10), 546–550 (2009)
- Williams, B.J., Santner, T.J., Notz, W.I.: Sequential design of computer experiments to minimize integrated response functions. *Stat. Sin.* **10**, 1133–1152 (2000)

**Publisher's Note** Springer Nature remains neutral with regard to jurisdictional claims in published maps and institutional affiliations.